

## Supplementary Material

### Efficient molecular oxygen utilization of micelle-based BiOCl for enhanced in situ H<sub>2</sub>O<sub>2</sub> production induced photocatalytic removal of antibiotics

Xiaojuan Bai<sup>\*a,b</sup>, Tianqi Jia<sup>a,b</sup>, Haiyan Li<sup>a,b</sup>, Linlong Guo<sup>a,b</sup>, Meipeng Jian<sup>a,b</sup>, Yongwei Gong<sup>a,b</sup>, Junqi Li<sup>a,b</sup>, Zhen Wei<sup>c</sup>, Derek Hao<sup>\*d</sup>

<sup>a</sup> Beijing Energy Conservation & Sustainable Urban and Rural Development Provincial and Ministry Co-construction Collaboration Innovation Center, Beijing University of Civil Engineering and Architecture, Beijing, 100044, China.

<sup>b</sup> Key Laboratory of Urban Stormwater System and Water Environment (Beijing University of Civil Engineering and Architecture), Ministry of Education, Beijing 100044, China

<sup>c</sup> Department of Chemistry, The University of Hong Kong

<sup>d</sup> Centre for Catalysis and Clean Energy, Gold Coast Campus, Griffith University, Gold Coast, 4222 Australia

#### 1. Experimental Procedures

##### Synthesis of materials

##### Materials

Bismuth nitrate pentahydrate [Bi(NO<sub>3</sub>)<sub>3</sub>·5H<sub>2</sub>O], Sodium chloride (NaCl), potassium bromide (KBr) potassium iodide (KI) and Anhydrous ethanol were purchased from Sinopharm Chemical Reagent Co., Ltd., Shanghai, China. Saponin powder was available from Xi 'an Chengtai Biotechnology Co., Ltd. (Shanxi, China).

##### Synthesis of BiOCl

2 mmol Bi(NO<sub>3</sub>)<sub>3</sub>·5H<sub>2</sub>O (0.970 g) and 2mmol of NaCl (0.116 g) were fitted into 100 ml beaker and dissolved in 70 ml deionized water and 10 ml ethanol, and then fully stirred for 30 min. Subsequently, the solution was injected into 150 ml Teflon liner and

heated at 160 °C for 18 h. After the mixed solution was cooled at room temperature, the suspension was washed several times with deionized water and ethanol until the upper solution was clarified. Then, the cleaned sample was dried in a vacuum oven at 70 °C. The samples were obtained by grinding, which was named as BiOCl.

### **Synthesis of BiOX (X = Br, I)**

2 mmol of  $\text{Bi}(\text{NO}_3)_3 \cdot 5\text{H}_2\text{O}$  and 2 mmol of KBr were dissolved in 10 ml of ethanol and 70 ml deionized water through strong stirring for 30 min. Then, the solution was transferred to 150 ml Teflon-lined autoclave and heated at 160 °C for 18 h. After cooling down to room temperature, the precipitate was washed with ethanol and deionized water by centrifuge several times and dried at 70 °C in vacuum. The sample was named BiOBr. Similarly, by changing KBr into 2 mmol of KI, the sample was named BiOI.

### **Synthesis of SA-BiOX (X = Br, I)**

Similar to SA-BiOCl, change NaCl into 2 mmol of KBr and KI, the sample was named SA-BiOBr and SA-BiOI. Other steps are the same as SA-BiOCl.

### **Theoretical calculation method**

We have employed the Vienna Ab initio Simulation Package (VASP) to perform all density functional theory (DFT) calculations within the generalized gradient approximation using the Perdew-Burke-Ernzerhof functional. We have chosen the projected augmented wave potentials to describe the ionic cores and take valence electrons into account using a plane-wave basis set with a kinetic energy cutoff of 400 eV. Geometry optimizations were performed with the force convergency smaller than 0.05 eV/Å. The atoms of single-layer BiOCl are relaxed, and atoms at bottom of double-layer BiOCl are fixed in all the calculations. Monkhorst-Pack k-points of  $2 \times 2 \times 1$  were applied for all the calculations.

## **2. Characterization**

The structure was observed by HT7700 transmission electron microscopy (TEM) and SU-8000 scanning electron microscopy (SEM), which were produced in Japanese Hitachi. Crystal phase characteristics of samples were gained by X-ray diffraction (XRD) analysis and high-resolution TEM (HRTEM) with PHI Quantera (Bruker, Germany) and JEM-2010F (JEOL, Japan). It used a VERTEX 70 (Bruker, Germany) to gain the Fourier transformed infrared (FTIR) to define the functional group. X-ray photoelectron spectroscopy (XPS) analyses and electron paramagnetic resonance (EPR) patterns were performed on VG ESCALAB MKII (Thermo, America) spectrometer and Bruker EMX PLUS spectroscopy (Bruker, Germany) to authenticate and study the existence of vacancies. Raman spectra were tested to grasp the composition of samples by LabRam HR Evolution (HORIBA, France), where it was operated with 532 nm. Photoluminescence (PL) spectra was analyzed by FP-6500 (JASCO, Japan) to gain the charge coincidence characteristics. The UV–Vis diffuses reflectance spectra (DRS) of samples were conducted by Lambda 650S (American) to investigate optical absorption properties. The Brunauer-Emmett-Teller (BET) surface was measured by TriStar II 3020 N<sub>2</sub> adsorption-desorption instrument (Micromeritics, America). The electrochemical impedance and photocurrent response were performed by the CHI-660E electrochemical workstations (CH Instruments, China) with 0.1 M Na<sub>2</sub>SO<sub>4</sub> aqueous solution.

### **3. Photocatalytic H<sub>2</sub>O<sub>2</sub> production**

Typically, 50 mg of catalyst was added into 50 ml aqueous solution in a container with mixing under the condition of avoiding light for 30 min before photoirradiation. During the whole reaction, 2 ml of the suspension was taken from the container every 30 min continuing 4 times. The amount of H<sub>2</sub>O<sub>2</sub> was measured by iodometry. The amount of H<sub>2</sub>O<sub>2</sub> in solution was determined by spectrophotometric method via a UV-Vis spectrophotometer at 350 nm<sup>1</sup>.

### **4. Photocatalytic activity evaluation**

#### **4.1 Photocatalytic degradation of MB**

25 mg catalyst was added into 50 ml of 5 ppm MB solution in a quartz glass tube and ultrasonically dispersed for 30 min in the dark. Meanwhile, 25 mg catalyst, 25 ml of 5 ppm MB solution and 25 ml of 1mM H<sub>2</sub>O<sub>2</sub> were added to the other quartz glass tube for degradation experiments. Before irradiation, the mixture was stirred in the dark for 30 min to reach the adsorption-desorption equilibrium. 1.5 ml of solution was taken out at stated intervals and centrifuged to remove the catalyst. The MB samples were purified by 0.45 μm PEFT membrane and analyzed by a UV-Vis spectrophotometer at 633 nm. As to light reaction, the illuminants of visible light (32.6 mA/cm<sup>2</sup>) were LED light (Beijing Perfectlight Co. Ltd.) with the wavelength longer than 420 nm, and 300 W Xe lamp.

#### **4.2 Photocatalytic degradation of DCF**

25 mg catalyst was added into 50 ml of 5 ppm DCF solution in a quartz glass tube and ultrasonically dispersed for 30 min in the dark. Before irradiation, the mixture was stirred in the dark for 30 min to reach the adsorption-desorption equilibrium. 1.5 ml of solution was taken out at stated intervals and centrifuged to remove the catalyst. The DCF samples were purified by 0.22 μm PEFT membrane and analyzed by Acquity UPLC H-Class (Waters, America). Mobile phases consisting of MeOH and 1% formic acid solution (65: 35, v/v) with a flow rate of 0.3 ml/min were used with a UV detector operating at 265 nm. As to light reaction, the illuminants of visible light (32.6 mA/cm<sup>2</sup>) were LED light (Beijing Perfectlight Co. Ltd.) with the wavelength longer than 420 nm, and 300 W Xe lamp.

#### **4.3 Photocatalytic degradation of antibiotics**

25 mg catalyst was added into 50 ml of 5 ppm antibiotics solution in a quartz glass tube and ultrasonically dispersed for 30 min in the dark. Before irradiation, the mixture was stirred in the dark for 30 min to reach the adsorption-desorption equilibrium. 1.5 ml of solution was taken out at stated intervals and centrifuged to remove the catalyst. The efficiency of the degradation of the antibiotics was measured by Acquity UPLC H-Class (Waters, America). The mobile phases of sulfanilamide and SMX consisted of

MeOH and 0.1% formic acid solution (60: 40, v/v) with a flow rate of 0.3 ml/min and were used with a UV detector operating at 270 nm. The mobile phases of acyclovir consisted of 0.05 mol/L Potassium dihydrogen phosphate solution and acetonitrile (82: 18, v/v) with a flow rate of 0.3 ml/min were used with a UV detector operating at 251 nm.

## 5. Results and Discussion

**Table S1.** The BET information of as-prepared samples.

Samples	BET Surface Area ( $\text{m}^2\cdot\text{g}^{-1}$ )	Pore Volume ( $\text{cm}^3\cdot\text{g}^{-1}$ )	Pore Size (nm)
BiOCl	3.31	0.013	8.41
SA-BiOCl	23.91	0.0089	11.33

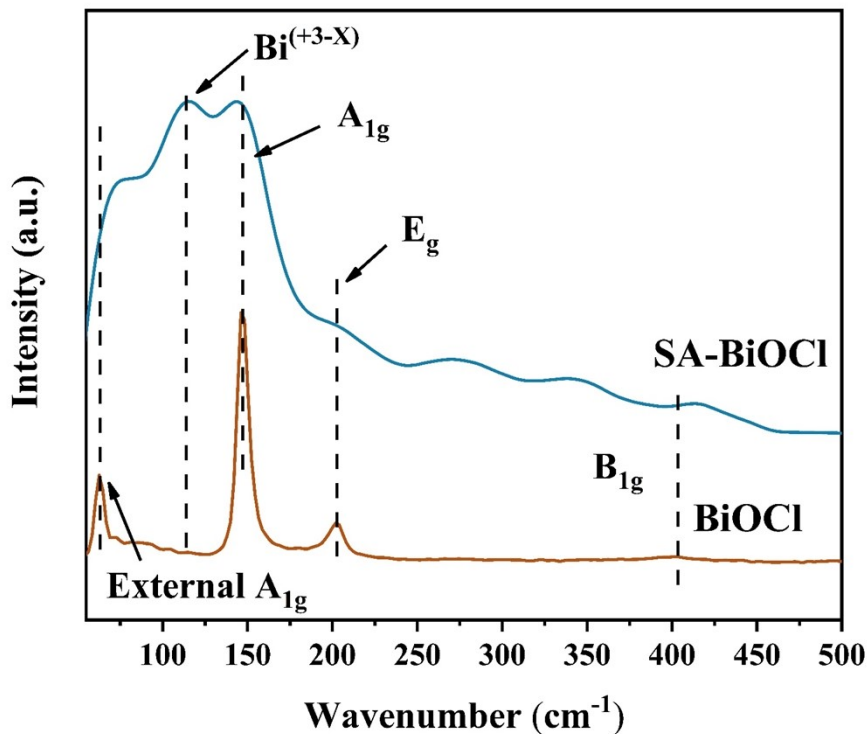


**Fig. S1.** Raman spectrum of BiOCl and SA-BiOCl samples.

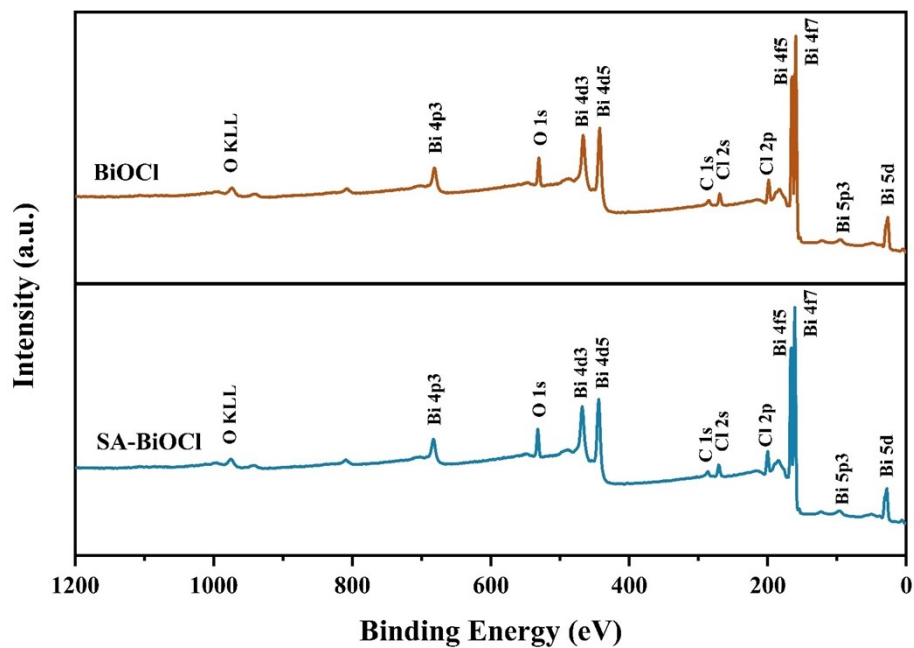


Fig. S2. XPS survey spectrum of BiOCl and SA-BiOCl samples.

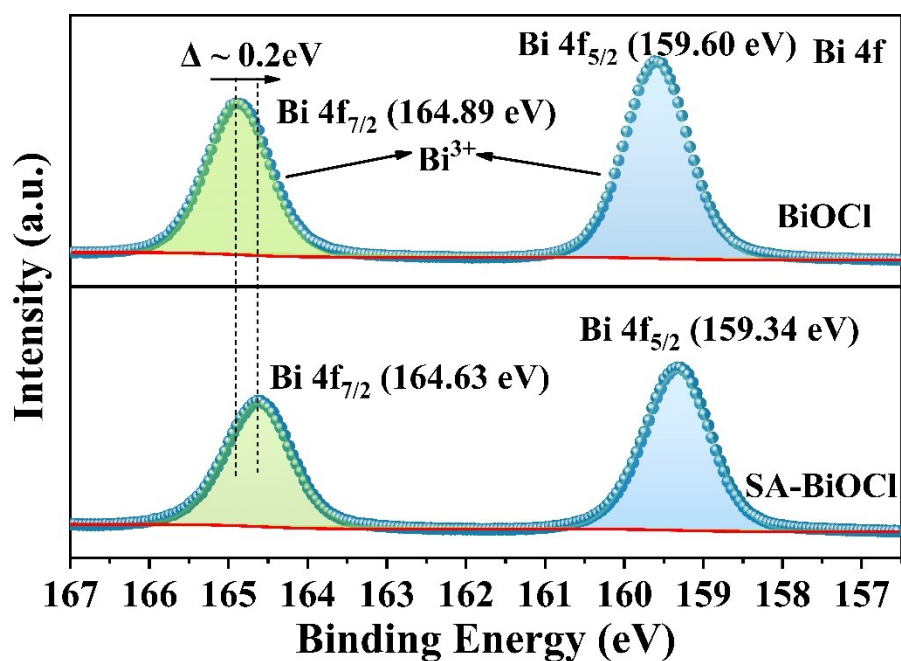
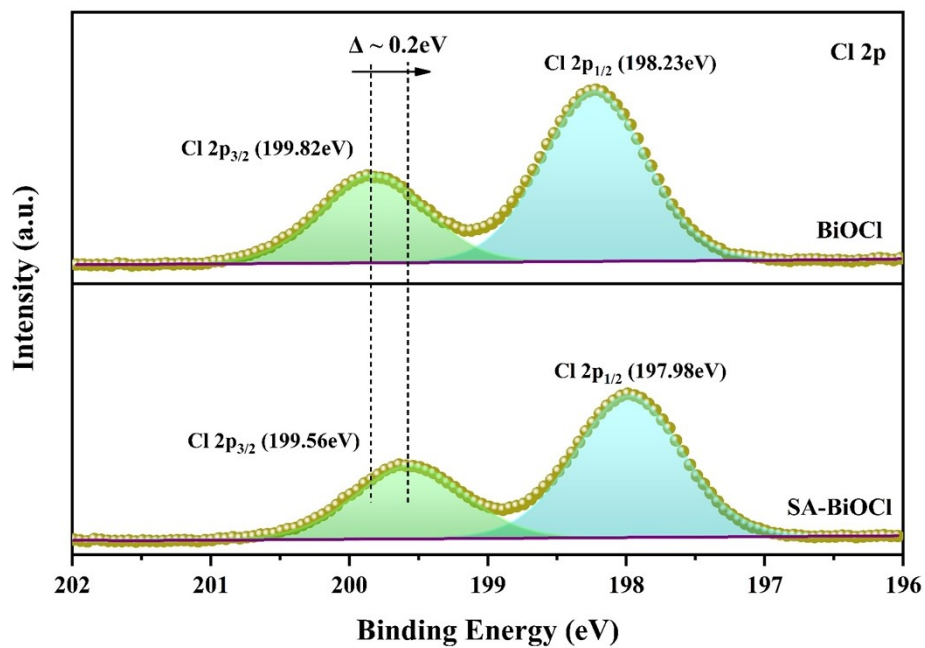
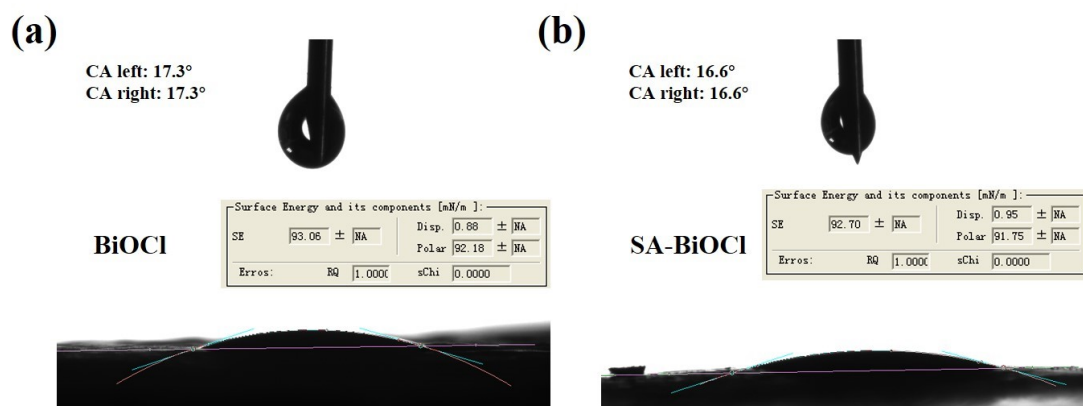


Fig. S3. The Bi 4f XPS spectra of BiOCl and SA-BiOCl samples.



**Fig. S4.** The Cl 2p XPS spectra of BiOCl and SA-BiOCl samples.



**Fig. S5.** The contact angle of (a) BiOCl and (b) SA-BiOCl.

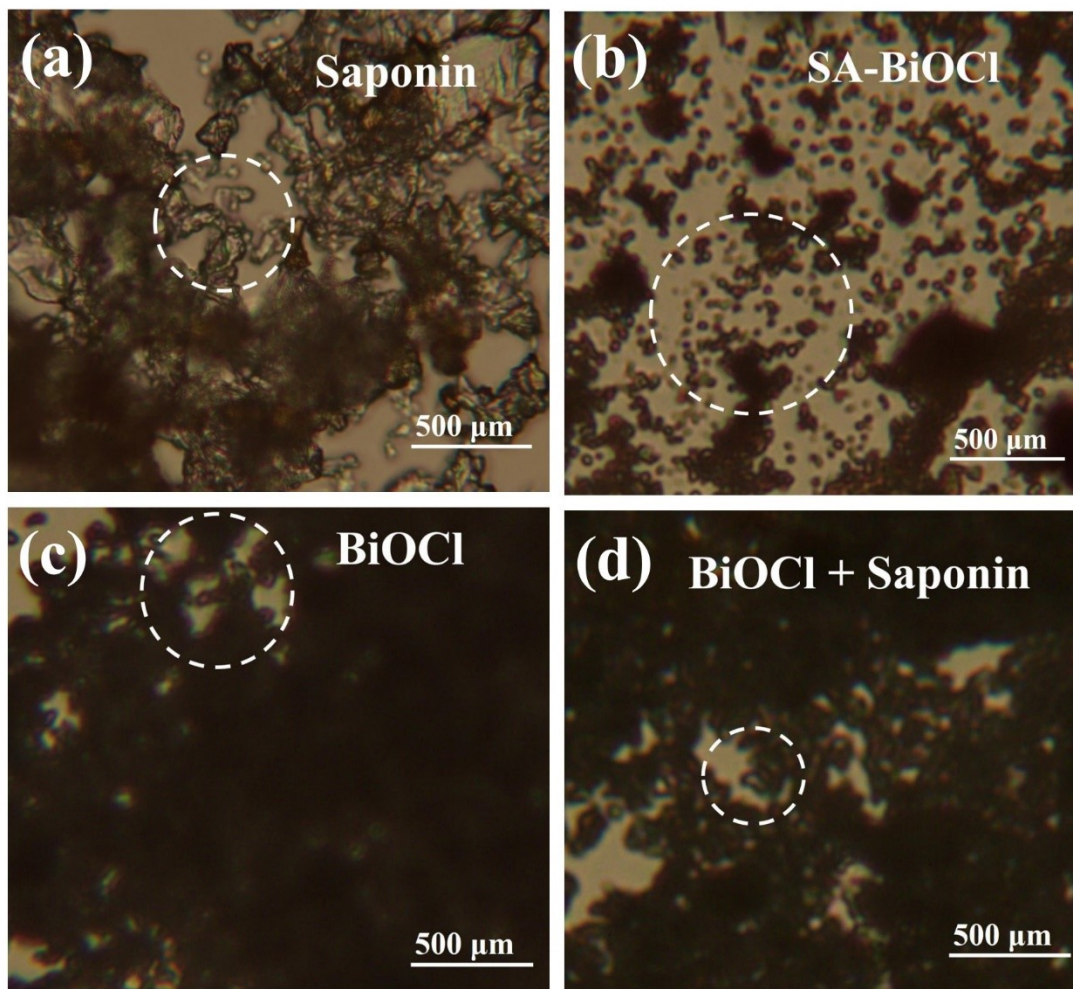


**Fig. S6.** Optical microscope image of (a) BiOCl, (b) SA-BiOCl, (c) BiOCl with saponin powder added, and (d) saponin powder.

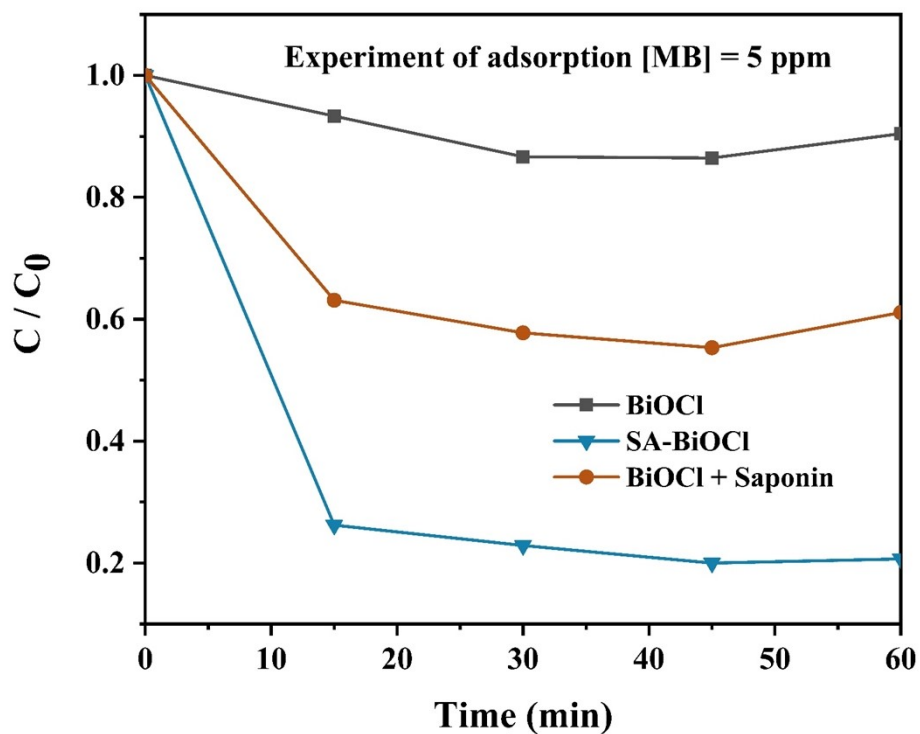


Fig. S7. Adsorption experiment of MB in dark.

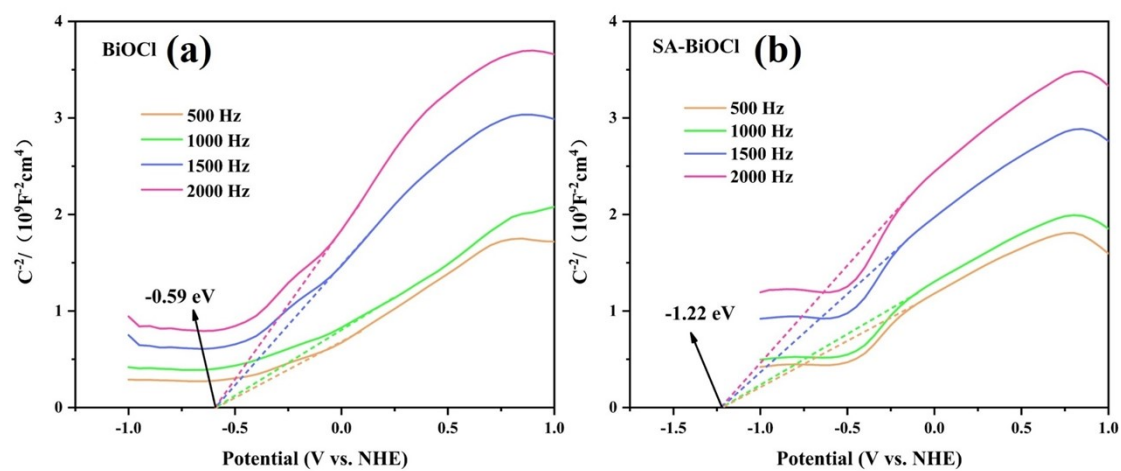


Fig. S8. Mott-schottky of (a) BiOCl and (b) SA-BiOCl samples.

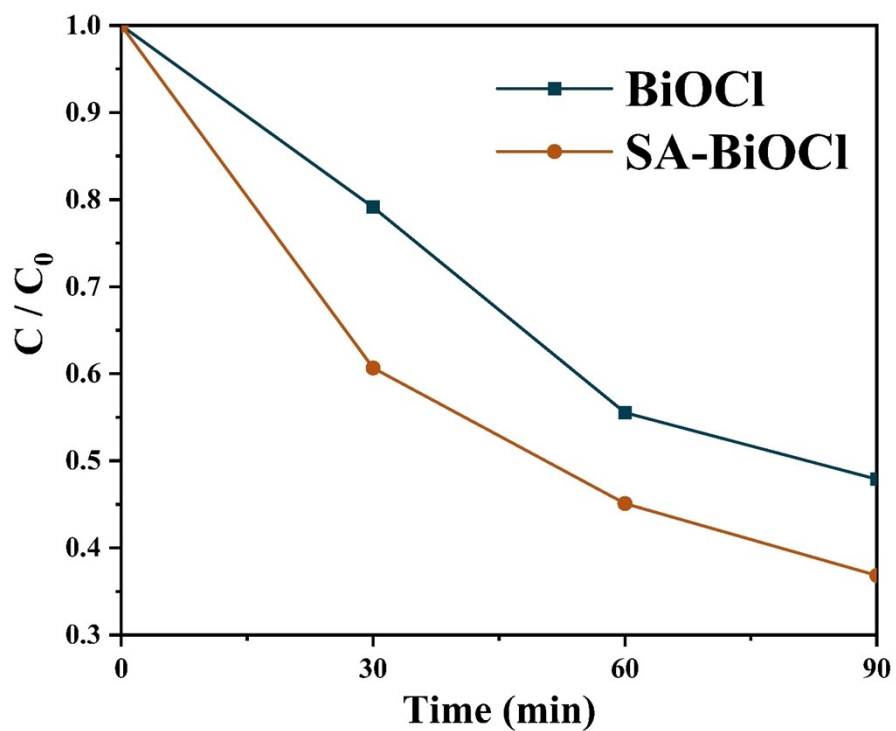


Fig. S9. The photocatalytic decomposition of H<sub>2</sub>O<sub>2</sub>.

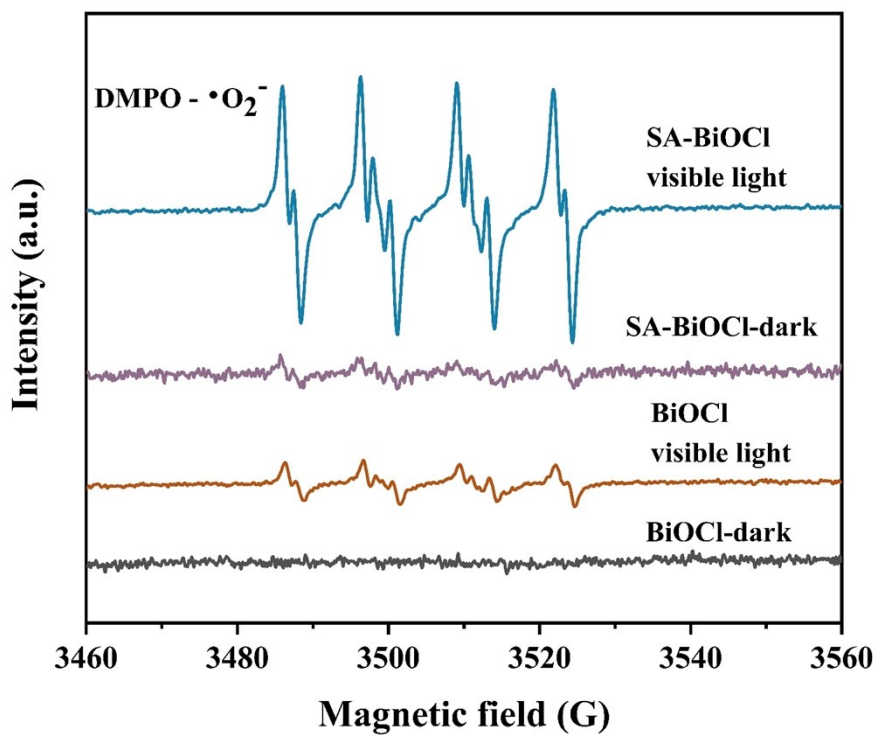


Fig. S10. EPR spectra of (h) DMPO - •O<sub>2</sub><sup>-</sup>.

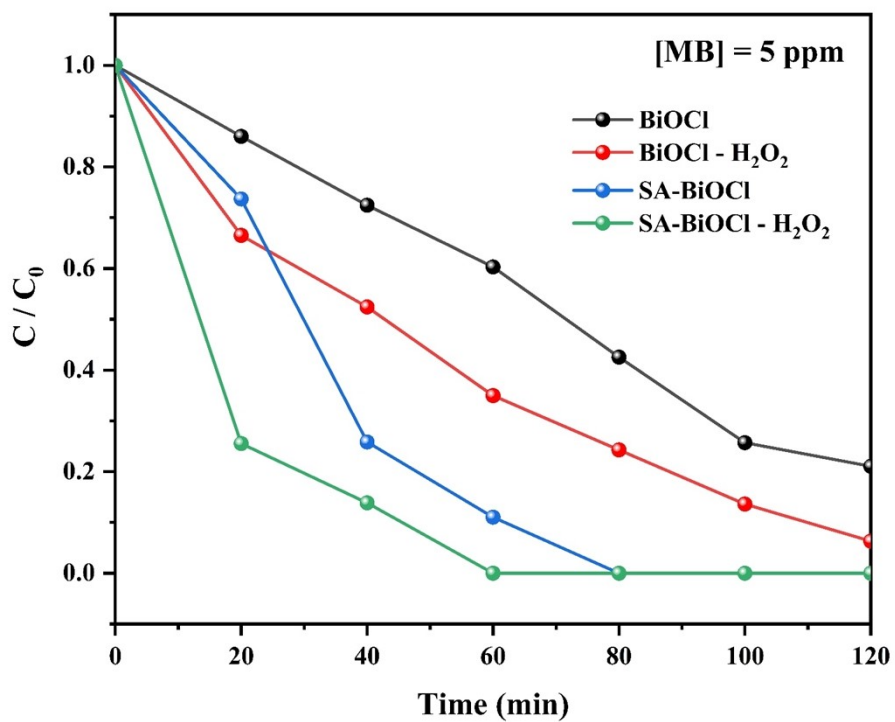


Fig. S11. Photocatalytic degradation of MB with additional H<sub>2</sub>O<sub>2</sub>.

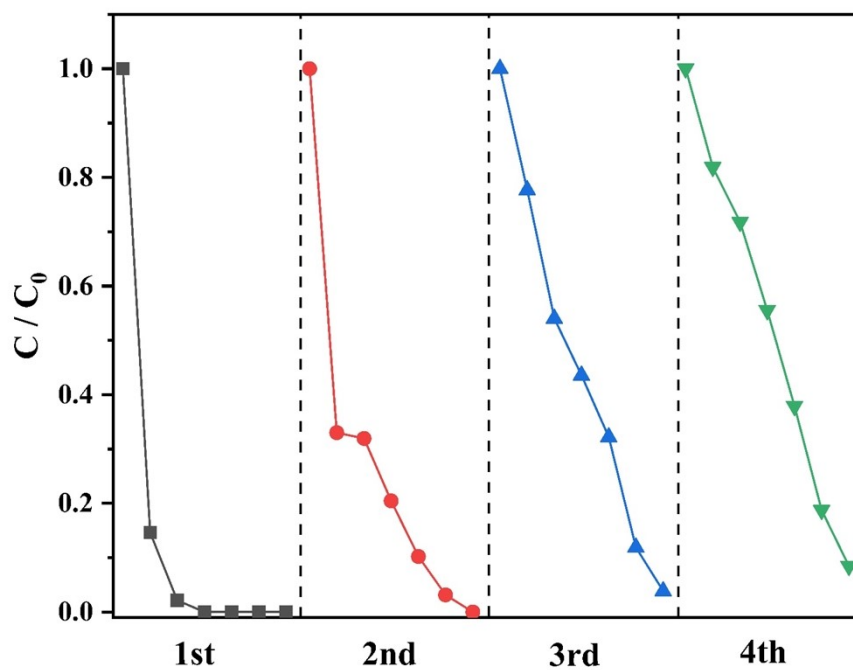


Fig. S12. Photocatalytic degradation of DCF by SA-BiOCl in four consecutive runs.

## 6. Method expansions

Inspired by the SA-BiOCl, we extended this method to other halogen atoms ( $X = \text{Br}$ ,  $\text{I}$ ). SA-BiOBr and SA-BiOI were synthesized by adding KBr and KI into the precursor solution. Similar to BiOCl, the XRD patterns (**Fig. S13**, **Fig. S14**) of the synthesized materials were comparable to those of their standard cards (BiOBr: JCPDS No. 09-0393, BiOI: JCPDS No. 10-0445), and no significant changes in the crystal structure were observed. At the same time, the change of diffraction peak also indicates the growth plane of the crystal. FT-IR and Raman spectra showed that the active groups of SA-BiOBr and SA-BiOI increased relative to the surface of the pristine samples, showing functional groups similar to BiOCl (**Fig. S15**). SEM, TEM and HRTEM images of BiOBr, BiOI, SA-BiOBr and SA-BiOI showed that the size of nanosheets decreases and the specific surface area increases after self-assembly induced by biosurfactant (**Fig. S16**). As can be seen from **Fig. S17**, the  $\text{N}_2$  adsorption/desorption isotherms of BiOBr, BiOI, SA-BiOBr and SA-BiOI belong to type IV isotherms, and the obvious hysteresis loops prove the existence of mesoporous structures. Meanwhile, the pore distribution curves of SA-BiOBr and SA-BiOI confirm that there are numerous micropore structures below 10 nm on the surface. SEM mapping analysis indicated that all samples were evenly distributed without the introduction of other elements (**Fig. S18**, **Fig. S19**). Due to the introduction of biosurfactant, the color of the sample also increased, and the absorption range of visible light increased significantly (**Fig. S20**). Their photocatalytic activity was evaluated by the degradation of pollutants. As shown in **Fig. S21**, the degradation rate of SA-BiOBr to DCF and sulfanilamide was increased by 1.35 and 1.18 times, respectively. In addition, the degradation rate of SA-BiOI to DCF and sulfanilamide was increased by 1.01 and 1.70 times, respectively. This is achieved by increasing the light absorption capacity and decreasing the surface free energy of amorphous metal oxides. The above results show that it is an effective method to modify BiOCl with a biosurfactant.

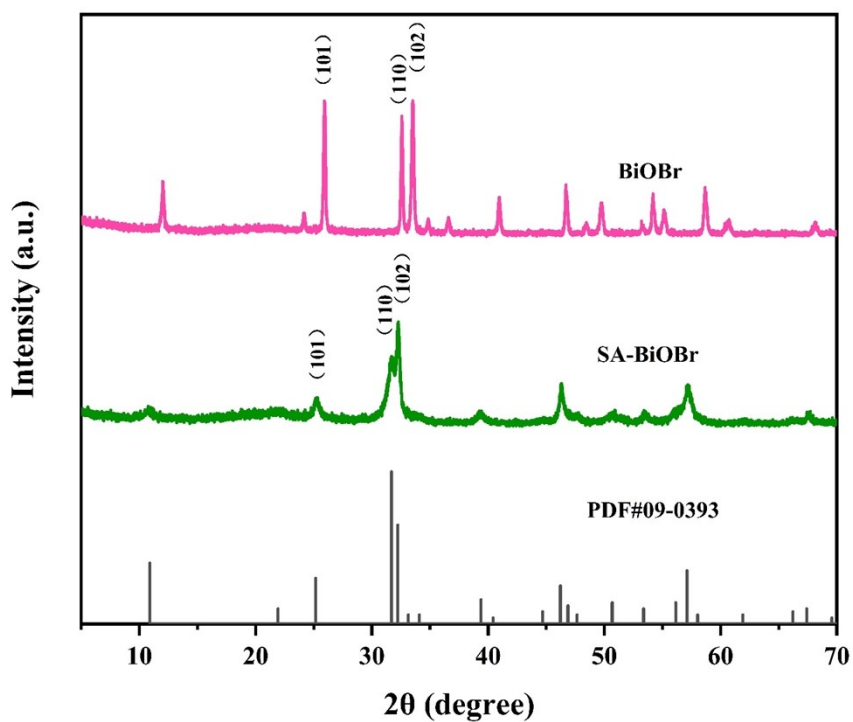


Fig. S13. XRD patterns of BiOBr and SA-BiOBr.

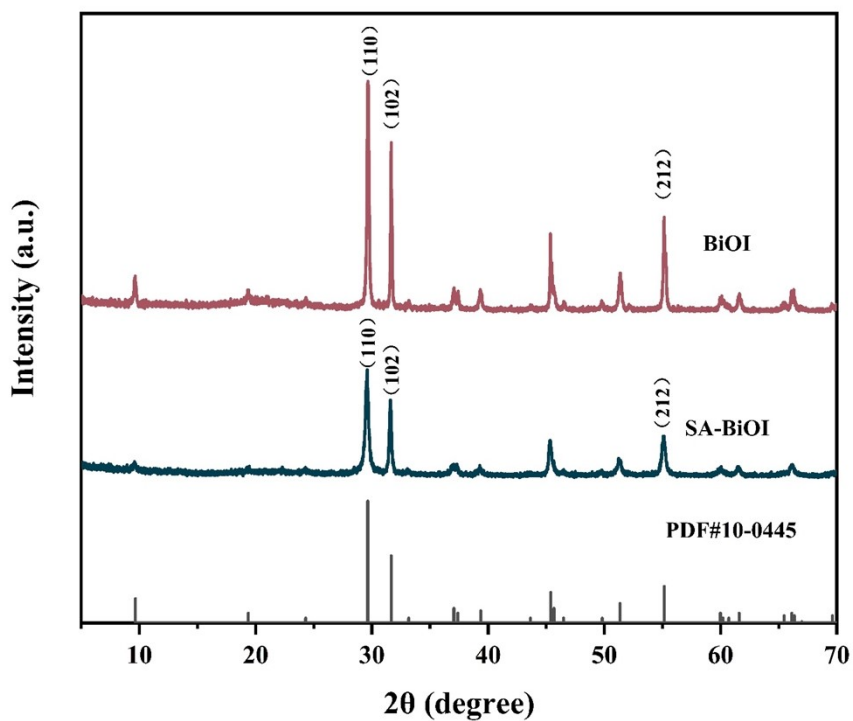
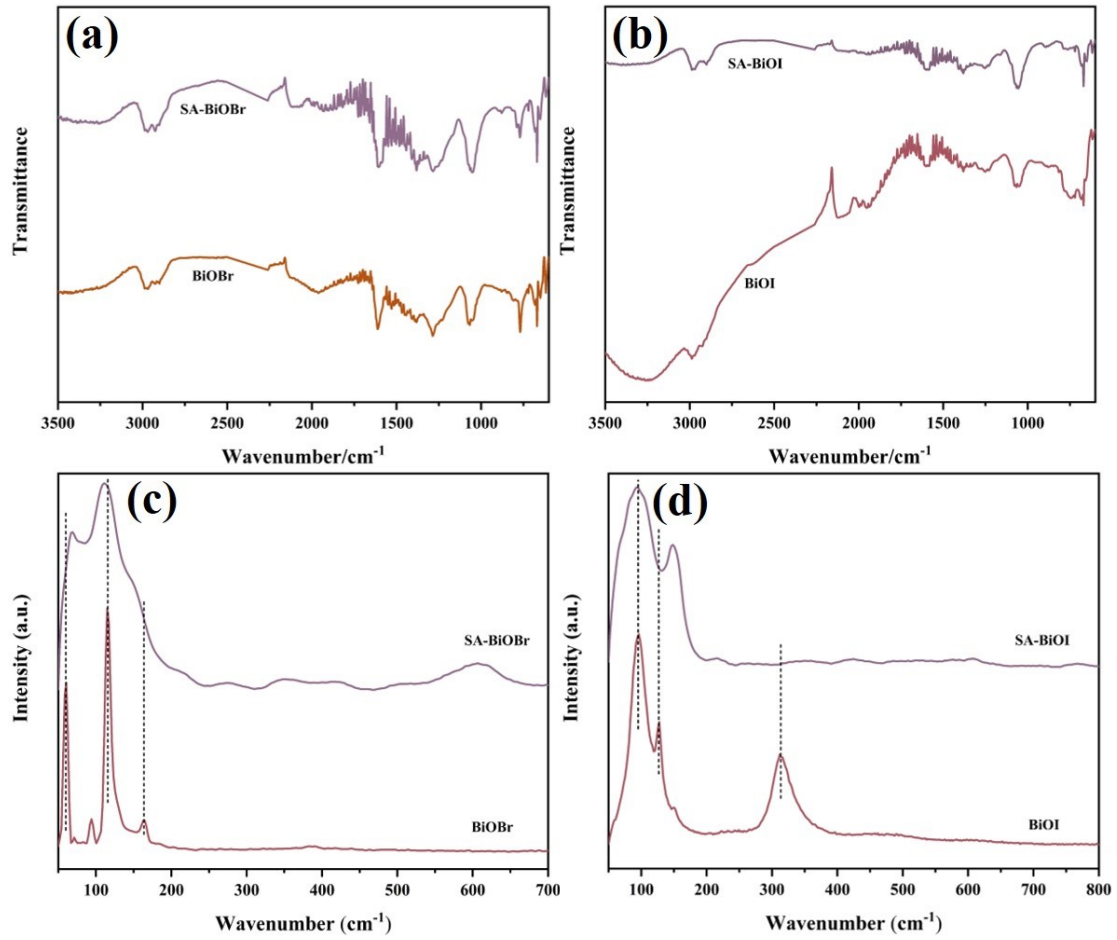
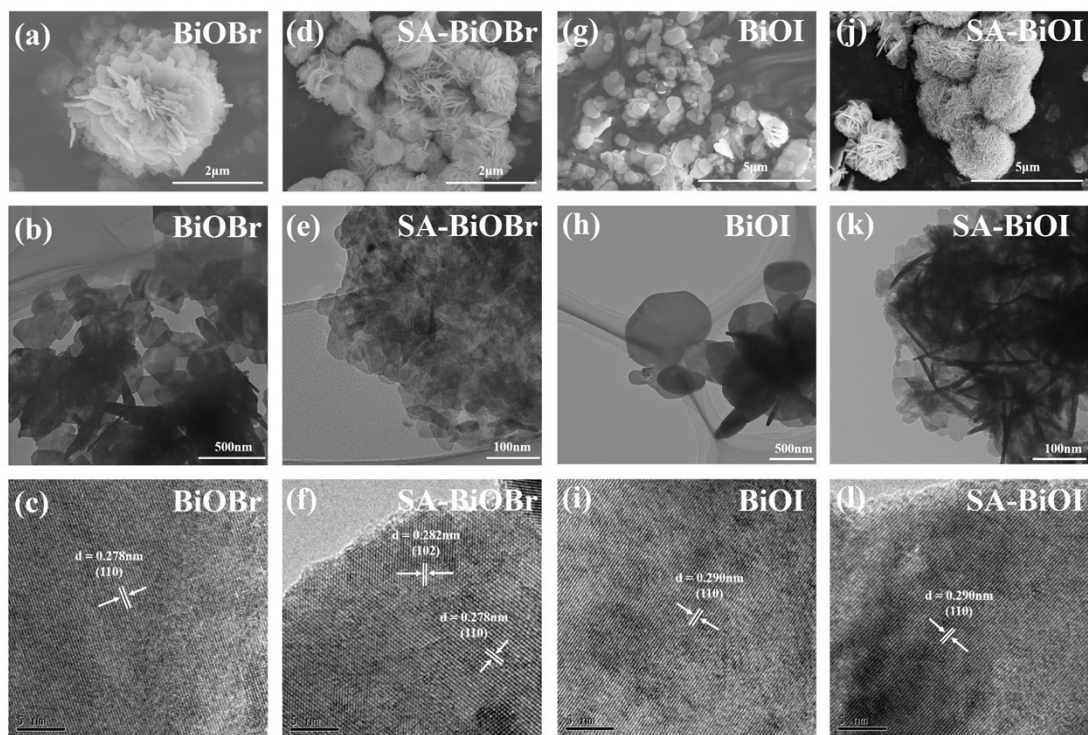


Fig. S14. XRD patterns of BiOI and SA-BiOI.



**Fig. S15.** FT-IR spectra of (a) BiOBr, SA-BiOBr and (b) BiOI, SA-BiOI; (c) Raman spectra of (c) BiOBr, SA-BiOBr and (d) BiOI, SA-BiOI.



**Fig. S16.** SEM images of (a) BiOBr, (d) SA-BiOBr, (g) BiOI, (j) SA-BiOI, TEM images of (b) BiOBr, (e) SA-BiOBr, (h) BiOI, (k) SA-BiOI, HRTEM images of (c) BiOBr, (f) SA-BiOBr, (i) BiOI, (l) SA-BiOI.

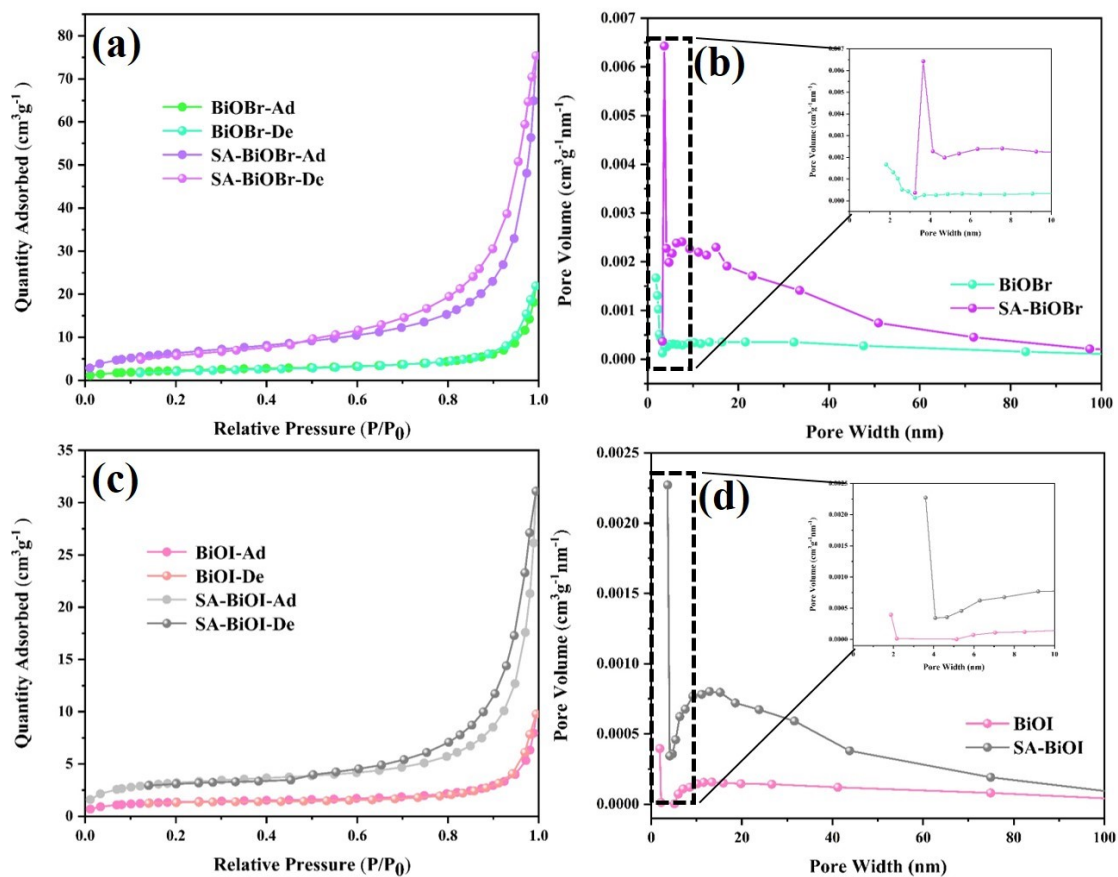


**Fig. S17.** (a) BET and (b) pore distribution of BiOBr and SA-BiOBr samples; (c) BET and (d) pore distribution of BiOI and SA-BiOI samples.

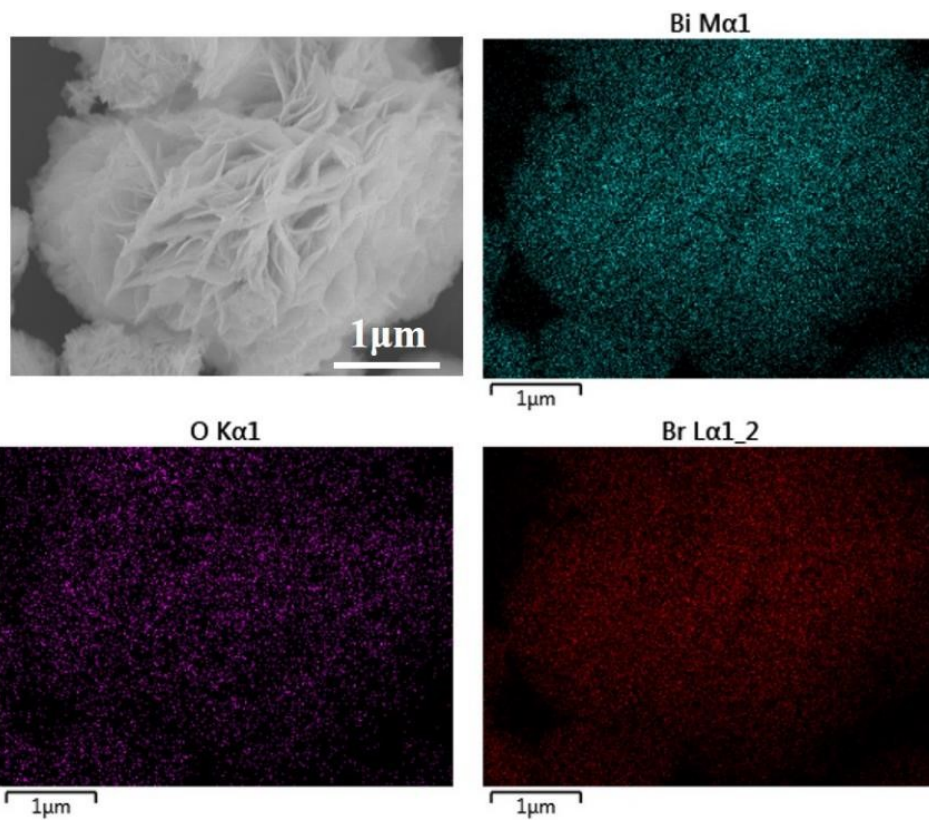


**Fig. S18.** SEM mapping images of SA-BiOBr.

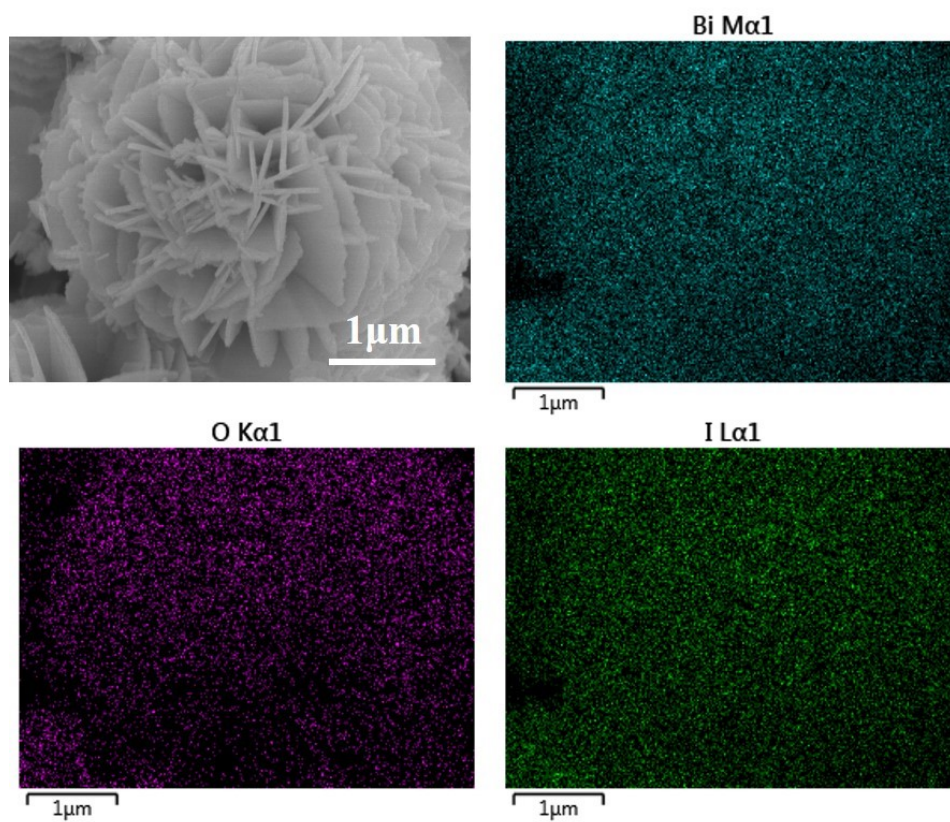


**Fig. S19.** SEM mapping images of SA-BiOI.

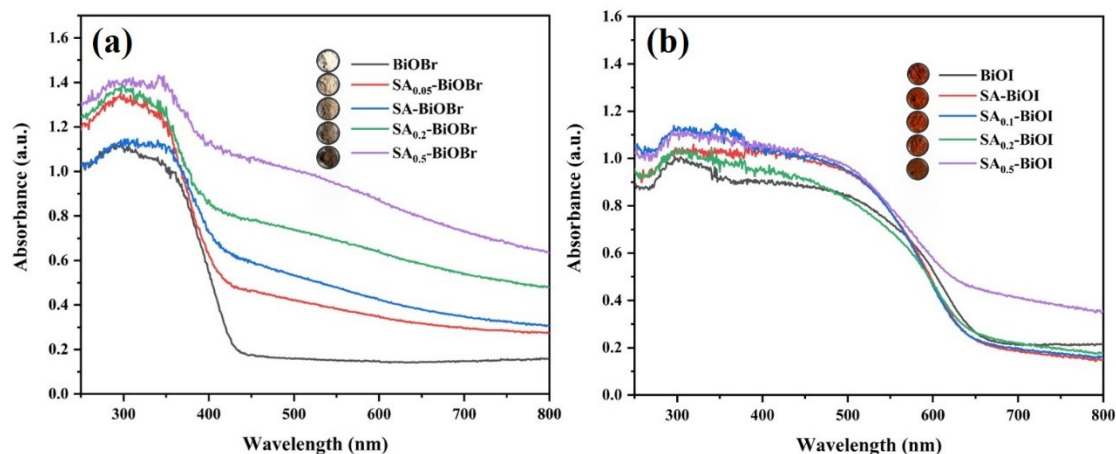


**Fig. S20.** DRS and optical images of different biosurfactant oxides modified (a) BiOBr and (b) BiOI.

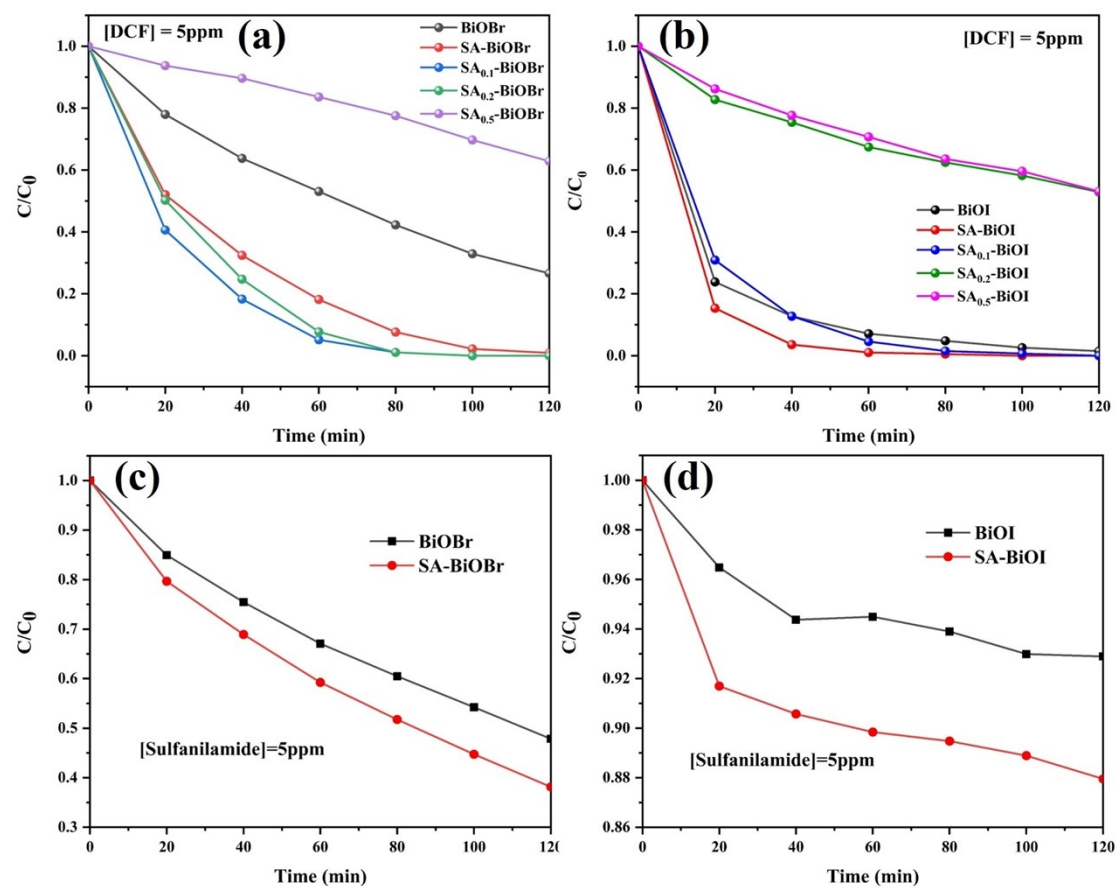


**Fig. S21.** Photodegradation of antibiotics in the presence of different catalysts under visible light ( $\lambda > 420$  nm)

## References

1. Z. Wei, M. Liu, Z. Zhang, W. Yao, H. Tan, Y. Zhu, Efficient visible-light-driven selective oxygen reduction to hydrogen peroxide by oxygen-enriched graphitic

carbon nitride polymers, *Energy Environ. Sci.* 2018, **11**, 2581-2589.